

Multi-task Bioassay Pre-training for Protein-ligand Binding Affinity Prediction

Jiaxian Yan^{1,2*}, Zhaofeng Ye^{2*}, Ziyi Yang², Chengqiang Lu¹,
Shengyu Zhang², Qi Liu^{1†}, Jiezhong Qiu^{2†}

¹University of Science and Technology of China, ²Tencent Quantum Laboratory
†qiliuql@ustc.edu.cn; jiezhongqiu@outlook.com

Abstract

Protein-ligand binding affinity (PLBA) prediction is the fundamental task in drug discovery. Recently, various deep learning-based models predict binding affinity by incorporating the three-dimensional structure of protein-ligand complexes as input and achieving astounding progress. However, due to the scarcity of high-quality training data, the generalization ability of current models is still limited. In addition, different bioassays use varying affinity measurement labels (i.e., IC50, Ki, Kd), and different experimental conditions inevitably introduce systematic noise, which poses a significant challenge to constructing high-precision affinity prediction models. To address these issues, we (1) propose *Multi-task Bioassay Pre-training* (MBP), a pre-training framework for structure-based PLBA prediction; (2) construct a pre-training dataset called ChEMBL-Dock with more than 300k experimentally measured affinity labels and about 2.8M docked three-dimensional structures. By introducing multi-task pre-training to treat the prediction of different affinity labels as different tasks and classifying relative rankings between samples from the same bioassay, MBP learns robust and transferrable structural knowledge from our new ChEMBL-Dock dataset with varied and noisy labels. Experiments substantiate the capability of MBP as a general framework that can improve and be tailored to mainstream structure-based PLBA prediction tasks. To the best of our knowledge, MBP is the first affinity pre-training model and shows great potential for future development. All codes and data are available on the online platform <https://github.com/jiaxianyan/MBP>.

1 Introduction

Protein-ligand binding affinity (PLBA) is a measurement of the strength of the interaction between a target protein and a ligand drug [1]. Accurate and efficient PLBA prediction is the central task for the discovery and design of effective drug molecules *in silico* [2]. Traditional computer-aided drug discovery tools use scoring functions (SF) to estimate PLBA roughly [3], which is of low accuracy. Molecular dynamics simulation methods can achieve more accurate binding energy estimation [4], but these methods are typically expensive in terms of computational resources and time. In recent years, deep learning (DL) models have been widely used to predict PLBA, which are thought to be promising tools for accurately and rapidly predicting PLBA. Based on the accumulated biological data, a series of DL-based scoring functions have been built, such as Pafnucy [5], OnionNet [6], Transformer-CPI [7], IGN [8], and SIGN [9]. In particular, structure-based DL models that use the 3D structure of protein-ligand complexes as inputs are most successful, which typically use 3D convolutional neural networks (3D-CNNs) [10; 11; 12] or graph neural networks (GNNs) [8; 9] to model and extract the interactions within the protein-ligand complex structures. However, the generalizability of these data-driven DL models is limited because the number of high-quality samples in PDBbind used for model training is relatively small (approximately 5,000) [13].

*These authors contribute equally to this work.

†Corresponding Authors.

One solution for this problem is pre-training, which has been widely used in computational biology, such as molecular pre-training for compound property prediction [14; 15; 16; 17] and protein pre-training for protein folding [18; 19; 20; 21]. These pre-training models utilize data from large-scale datasets to learn embeddings, which expand the ligand chemical space and protein diversities. Therefore, affinity pre-training models on the large amount of affinity data in databases such as ChEMBL [22] and BindingDB [23] can be helpful. Nevertheless, though attempts have been made to directly use the data, such as BatchDTA [24], several challenges have prevented researchers from widely using ChEMBL data for PLBA previously. Firstly, the data were collected from various bioassays, which introduce different system biases and noises to the data and make it difficult for comparison [24; 25] (**label noise problem**). For some cases, the affinities of the same protein-ligand pair in different bioassay can have a difference of several orders of magnitude (Fig. 1). Secondly, several types of affinity measurement exist (**label variety problem**), such as half-maximal inhibitory concentration (IC50), inhibition constant (Ki), inhibition ratio, dissociation constant (Kd), half-maximal effective concentration (EC50), etc., which cannot be compared directly as well. Thirdly, the unavailability of 3D structures of protein-ligand complexes within ChEMBL poses a significant limitation for researchers in training and leveraging structure-based DL models (**missing conformation problem**).

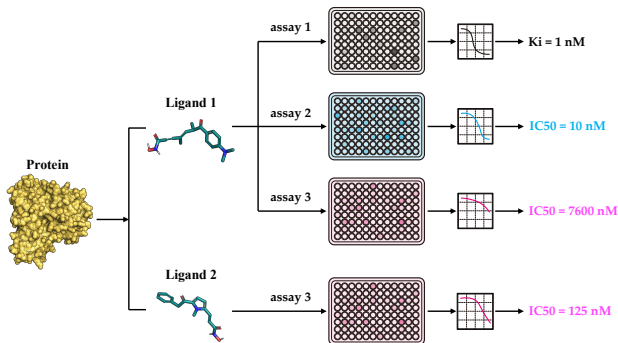


Figure 1: A real example of bioassay data in ChEMBL. (1) The top three panels show an example where the same protein-ligand pair have different binding affinities with assay 1-3 in terms of measurement type (IC50 v.s. Ki) and value (IC50=10 nM v.s. IC50=7600 nM). (2) The bottom two panels show an example of the binding of different ligands (Ligand 1 & 2) to a protein in the same assay (assay 3).

To solve the above problems, we propose the Multi-task Bioassay Pre-training (MBP) framework for structure-based PLBA prediction models. In general, by introducing multi-task and pairwise ranking within bioassay samples, MBP can make use of the noisy data in databases like ChEMBL. Specifically, the multi-task learning strategy [26] treats the prediction of different label measurement types (IC50/Ki/Kd) as different tasks, thus enabling information extraction from related but different affinity measurements. Meanwhile, although different assays can introduce different types of noises to the data, data from the same assay is relatively more comparable. Inspired by recent progress in the recommendation system [27; 28; 29], by considering ranking between samples from the same assay, the model is enforced to learn the relative relationship of samples and differences in protein-ligand interactions, which allows the MBP to learn robust and transferrable structural knowledge beyond the noisy labels.

We then construct a pre-training dataset, ChEMBL-Dock, for MBP. ChEMBL-Dock contains 313,224 protein-ligand pairs with from 21,686 assays and the corresponding experimental PLBA labels (IC50/Ki/Kd). Molecular docking softwares are employed to generate about 2.8M docked 3D complex structures in ChEMBL-Dock. Then we implant MBP with simple and commonly used GNN models, such as GCN [30], GIN [31], GAT [32], EGNN [33], and AttentiveFP [34]. Experiments on the PDBbind core set and the CSAR-HiQ dataset have shown that even simple models can be improved and achieve comparable or better performances than the state-of-the-art (SOTA) models with MBP. Through ablation studies, we further validate the importance of multi-task strategy and bioassay-specific ranking in MBP.

Overall, the contributions of this paper can be summarized as follows:

- We propose the first PLBA pre-training framework MBP, which can significantly improve the accuracy and generalizability of PLBA prediction models.
- We construct a high-quality pre-training dataset, ChEMBL-Dock, based on ChEMBL, which significantly enlarges existing PLBA datasets in terms of chemical diversities.
- We show that even vanilla GNNs can significantly outperform the previous SOTA method by following the pre-training protocol in MBP.

2 Related Work

Protein-Ligand Binding Affinity Prediction. One critical step in drug discovery is scoring and ranking the predicted protein-ligand binding affinity. Scoring functions can be roughly divided into four main types: force-field-based, empirical-based, machine-learning-based, and 3D-structure-based [9]. Force-field-based methods aim at estimating the free energy of the binding by using the first principles of statistical mechanics [6]. Despite its remarkable performance as a gold standard, it suffers from high computational overhead. Empirical-based methods [35; 36; 37] design docking and scoring functions especially to make affinity predictions, while expert domain knowledge is needed to encode internal biochemical interactions. Machine-learning-based methods, such as random forest [38] and support vector machines (SVM)[39], aim to predict binding affinity based on a data-driven learning paradigm. These methods, however, rely on the quality of hand-crafted features and have poor performance in generalization. Recently, due to advances in deep learning methods and the creation of structure-based protein-ligand complex datasets, many structure-based deep learning methods [40; 6; 41; 42; 15; 43; 44; 8; 9] have been developed for predicting binding affinity. Such methods directly learn the structural information of protein-ligand complexes end-to-end, avoiding artificial feature design. However, due to the scarcity of high-quality training data, current methods still suffer from poor generalization in real applications.

Datasets of Protein-Ligand Binding Affinity. Existing protein-ligand binding affinity datasets can be roughly divided into three categories. The first category includes datasets such as PDBbind, BindingMOAD [45], and CSAR-HIQ [46], which contain 3D co-crystal structures of protein-ligand complexes determined by structural characterization methods and experimentally determined binding affinity values. Such datasets have small yet high-quality data and are typically widely used for training structure-based deep learning models [47; 48]. The second category contains large-scale protein-ligand binding affinity measured labels but without 3D structures, such as ChEMBL and BindingDB. The third category contains the 3D structure and binding affinity value of the protein-ligand complex calculated by molecular docking [49], and the representative database is CrossDocked [50]. Due to the lack of experimental affinity labels, such datasets are often used to train generative models rather than affinity prediction models [51].

Pre-training for Biomolecules. Much effort has been devoted to biomolecular pre-training to achieve better performance on related tasks. For small molecules and proteins, a series of self-supervised pre-training methods based on molecular graphs [14; 15; 16; 17] and protein sequences [18; 19; 20; 21] have been proposed, respectively. However, these existing pre-training methods are designed for individual molecules [52], and there is still a gap in the research on pre-training methods for protein-ligand affinity.

Pairwise Learning to Rank. Learning to Rank (LTR) is an essential research topic in many areas, such as information retrieval and recommendation systems [53; 54; 55]. The common solutions of LTR could be basically categorized into three types: pointwise, pairwise, and listwise. Among these methods, pairwise LTR models are widely used in practice due to their efficiency and effectiveness. These years have witnessed the success of pairwise methods, such as BPR [56], RankNet [57], GBRank [58], and RankSVM [59]. In addition, recent studies have shown that the bias between labels can be effectively solved using pairwise methods [27].

3 Multi-Task Bioassay Pre-training

In this section, we formalize the problem of pre-training for PLBA and then introduce our proposed multi-task bioassay pre-training framework — MBP. After defining the problem, we provide a framework overview of our solution in Section 3.1. Then, in Section 3.2, we discuss how we develop a GNN-based model as the shared-bottom encoder in multi-task learning. Finally, we present the curation process of the ChEMBL-Dock dataset used for pre-training in Section 3.3.

Problem Formulation. Conceptually, given a protein P , a ligand L , and the binding conformation C of the ligand to the protein, the problem of structure-based protein-ligand binding affinity prediction is to learn a model $f(P, L, C)$ to predict the binding affinity. However, due to the rarity and high cost of ground truth 3D structure data, the training of structure-based PLBA prediction models has to be restricted to PDBbind with co-crystal structures. In this work, we aim to leverage the ChEMBL dataset, which contains large-scale protein-ligand binding affinity data but without 3D structures.

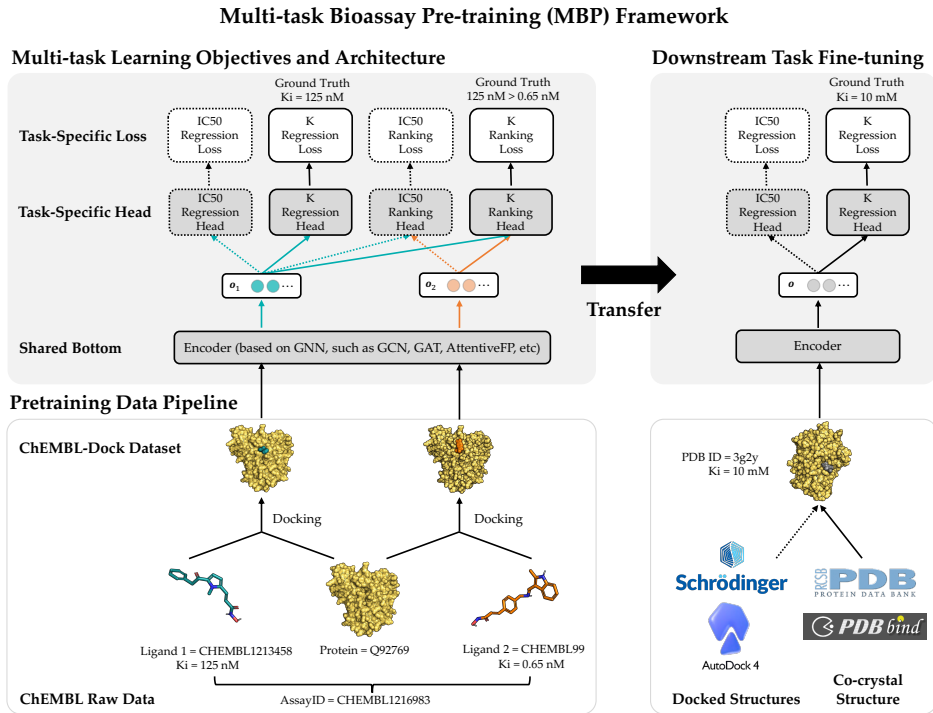


Figure 2: The framework of MBP in pre-training and fine-tuning. The solid arrows indicate the flow path of the running examples of AssayID = CHEMBL1216983 during pre-training and PDB ID = 3g2y during fine-tuning.

As discussed in Section 1, in order to pre-train a PLBA prediction model on ChEMBL, we have to resolve three challenges, namely label variety, label noise, and missing conformation.

3.1 Framework Overview

The framework overview of MBP is illustrated in Fig. 2, which includes three main parts — (1) pre-training data pipeline; (2) multi-task learning objectives and architecture; and (3) downstream task fine-tuning. In this section, we describe them in detail.

Pre-Training Data Pipeline. Before introducing the pre-training data pipeline, we provide the necessary definitions of a bioassay and a bioassay-specific data pair in MBP.

Definition 1 (A Bioassay in MBP). A bioassay is defined as an analytical method to determine the concentration or potency of a substance by its effect on living animals or plants (in vivo) or on living cells or tissues (in vitro) [60]. In this work, we mainly focus on bioassays measuring in vitro binding of ligands to a protein target. Formally, the i -th bioassay is denoted as

$$A_i = \left(P_i, \{ (L_{ij}, y_{ij}) \}_{j=1}^{n_i}, t_i \right). \quad (1)$$

It means that there are n_i experimental records in bioassay A_i , and each record measures the binding affinity y_{ij} of a ligand L_{ij} to the protein target P_i . And the type of binding affinity in bioassay A_i is t_i , in this work we consider $t_i \in \{Ki, Kd, IC50\}$. The ChEMBL dataset can be formalized as a collection of bioassays such that $\mathcal{D} = (A_1, A_2, \dots)$.

Definition 2 (A Bioassay-specific Data Pair). A bioassay-specific data pair is a six-tuple $(P_i, L_{ij}, L_{ik}, y_{ij}, y_{ik}, t_i)$, indicating there is a bioassay A_i which includes the binding measurement of ligand L_{ij} and ligand L_{ik} to a protein target P_i . And the experimentally measured binding affinity (with type t_i) is y_{ij} and y_{ik} , respectively.

The bioassay-specific data pairs in this work are extracted and randomly sampled from ChEMBL bioassays [22]. We first sample a bioassay A_i with probability proportional to its size, i.e., $\text{Prob}(A_i) \propto n_i$. Then we randomly pick two different ligands L_{ij} and L_{ik} from the sampled assay A_i , together with their binding affinity y_{ij} and y_{ik} . The above sampling process produces a bioassay-specific data pair $(P_i, L_{ij}, L_{ik}, y_{ij}, y_{ik}, t_i)$ as defined in Definition 2. Taking the running case shown in Fig. 2 as

an example, the data pair from a ChEMBL bioassay (with AssayId = ChEMBL1216983) can be written as (Q92769, ChEMBL1213458, ChEMBL99, 125nM, 0.65nM, Ki).

Knowledge of the binding conformation of a ligand to a target protein plays a vital role in structure-based drug design, particularly in predicting binding affinity. However, the ground truth co-crystal structure of a protein-ligand complex is experimentally very expensive to determine and is therefore not available in ChEMBL. Consequently, we only have the binding affinities (e.g., y_{ij} and y_{ik}) of a ligand to a protein without knowing their conformation and relative orientation. To solve the above missing data problem, we propose to use computationally determined docking poses as an approximation to the true binding conformations. Specifically, we construct a large-scale docking dataset named ChEMBL-Dock from ChEMBL. For each protein-ligand pair in ChEMBL, we generate its docking poses according to the following three steps. Firstly, we use RDKit library [61] to generate 3D conformations from the 2D SMILES of the ligand. Then, the 3D structure of a protein is extracted from PDBbind according to its UniProt ID. Finally, we use docking software SMINA [62] to generate the docking poses of the protein-ligand pair. Throughout the rest of this paper, we denote the docking conformation of protein P_i and ligand L_{ij} as C_{ij} . The detailed data curation process of ChEMBL-Dock can be found later in Section 3.3.

Overall, the pre-training data pipeline generates bioassay-specific data pairs $(P_i, L_{ij}, L_{ik}, y_{ij}, y_{ik}, t_i)$, retrieves their docking conformations — C_{ij} and C_{ik} — from the pre-processed ChEMBL-Dock datasets, and then feeds them into a multi-task learning model which we will discuss below.

Multi-task Learning Objectives and Architecture. As discussed in Section 1, there are three main challenges of applying pre-training to the PLBA problem — missing conformation, label variety, and label noise. In this section, we propose to solve the label variety and label noise problem via multi-task learning.

For the label variety challenge, it is intuitive and straightforward to introduce label-specific tasks for each type of binding affinity measurement. In this work, we define two categories of label-specific tasks — IC50 task and $K=\{Ki, Kd\}$ task, which handle bioassay data with affinity measurement type IC50 and Ki/Kd, respectively. Here we merge Ki and Kd as a single task following [63], and the main reasons are twofold. Firstly, Ki and Kd are calculated in the same way, except that Kd only considers the physical binding, while Ki specifies the biological effect of this binding to be inhibition. So they can essentially be seen as the same label type. Secondly, the number of Kd data is significantly less compared to Ki data, which may lead to data imbalance if we were to design a separate Kd task.

For the label noise challenge, instead of leveraging learning with noisy labels techniques [64], we turn to utilize the intrinsic characteristics of bioassay data. As discussed in Section 1, the label noise challenge in ChEMBL stems mainly from its data sources and curation process. The binding affinity values from different bioassays were measured under various experimental protocols and conditions (such as temperature and pH value), leading to systematic errors between different assays. However, the binding affinity labels within the same bioassay were usually determined under similar experimental conditions. Thus, intra-bioassay data are more consistent than inter-bioassay ones, and the comparison within a bioassay is much more meaningful. Inspired by the above characteristics of bioassay data, we design both regression tasks and ranking tasks in MBP. To be more formal, given a bioassay-specific data pair $(P_i, L_{ij}, L_{ik}, y_{ij}, y_{ik}, t_i)$, the regression task is to directly predict the binding affinity y_{ij} , while the ranking task is to compare the binding affinity values within the bioassay, i.e., to classify whether $y_{ij} < y_{ik}$ or $y_{ij} > y_{ik}$.

In summary, we have $2 \times 2 = 4$ tasks in MBP, namely the IC50 regression task, IC50 ranking task, K regression task, and K ranking tasks. An illustration of these tasks can be found in Fig. 2.

As for the multi-task learning architecture, we adopt the shared-bottom technique (also known as the hard parameter sharing) [65] in MBP. Such a technique shares a bottom encoder among all tasks while keeping several task-specific heads. As illustrated in Fig. 2, the model architecture consists of a shared encoder network f_{Enc} and four task specific heads — an IC50 regression head $f_{\text{IC50, Reg}}$, a $K=\{Ki, Kd\}$ regression head $f_{K, \text{Reg}}$, an IC50 ranking head $f_{\text{IC50, Rank}}$ and a $K=\{Ki, Kd\}$ ranking head $f_{K, \text{Rank}}$. Given a bioassay-specific data pair $(P_i, L_{ij}, L_{ik}, y_{ij}, y_{ik}, t_i)$ together with their conformation C_{ij} and C_{ik} from the pre-training data pipeline, the shared bottom encoder maps them into compact hidden representations shared among tasks:

$$\mathbf{o}_1 = f_{\text{Enc}}(P_i, L_{ij}, C_{ij}) \text{ and } \mathbf{o}_2 = f_{\text{Enc}}(P_i, L_{ik}, C_{ik}). \quad (2)$$

There are many possibilities for implementing an encoder for protein-ligand complexes, including but not limited to models based on 3D-CNN [66; 12; 50], GNN [67; 9; 8], and Transformer [68; 69; 7]. In MBP, we propose a simple and effective shared bottom encoder. For the sake of clarity, we defer its implementation detail in Section 3.2, and focus on multi-task learning in this section.

For the regression task, we pick the task-specific regression head $f_{t_i, \text{Reg}}$ according to the label type $t_i \in \{\text{IC50}, \text{K}\}$ (recall that Ki and Kd have been merged to be a single label type K), and predict the binding affinity to be $\hat{y}_{ij} = f_{t_i, \text{Reg}}(\mathbf{o}_1)$. The regression loss is calculated using the mean squared error (MSE) loss between ground truth y_{ij} and the predicted value \hat{y}_{ij} . More formally, the regression loss is defined as

$$L_{\text{Reg}} = \text{MSE}(\hat{y}_{ij}, y_{ij}). \quad (3)$$

It is worth mentioning that for a data pair, only label y_{ij} will be used to compute the regression loss.

Similarly, for the ranking task, we select the task-specific ranking head $f_{t_i, \text{Rank}}$ according to the label type $t_i \in \{\text{IC50}, \text{K}\}$, concatenate the hidden representations as $\mathbf{o}_1 || \mathbf{o}_2$, and then predict the pairwise ranking to be $\hat{r}_{ijk} = f_{t_i, \text{Rank}}(\mathbf{o}_1 || \mathbf{o}_2)$. The ranking loss is calculated as the binary cross entropy loss between ground truth $\mathbb{I}[y_{ij} > y_{ik}]$ and the predicted value \hat{r}_{ijk} , where $\mathbb{I}(\cdot)$ denotes the indicator function. More formally, the ranking loss is defined as

$$L_{\text{Rank}} = \text{BCE}(\hat{r}_{ijk}, \mathbb{I}[y_{ij} > y_{ik}]). \quad (4)$$

The overall loss function for a bioassay-specific data pair is a weighted sum of the regression loss in Equation 3 and ranking loss in Equation 4:

$$L_{\text{MBP}} = L_{\text{Rank}} + \lambda \times L_{\text{Reg}}, \quad (5)$$

where λ is the weight coefficient for regression loss.

Overall, we introduce multi-task learning into MBP, aiming to deal with label variety and label noise problems. In the illustrative example of MBP shown in Fig. 2, MBP accepts the bioassay-specific data pair (Q92769, ChEMBL1213458, ChEMBL99, 125nM, 0.65nM, Ki) and their docking poses as inputs, encodes them to hidden representations, forwards the K regression head to predict $y_{ij} = 125\text{nM}$, and also forward the K ranking head to classify $125\text{nM} > 0.65\text{nM}$.

Downstream Task Fine-Tuning. The final part of the MBP framework is the downstream task fine-tuning. Given the 3D structure of a protein-ligand complex as input, the downstream task is to predict its binding affinity. The 3D structure can be either an experimentally determined co-crystal structure or a computationally determined docking pose. We transfer and fine-tune the shared bottom encoder f_{Enc} together with the regression heads $f_{\text{IC50, Reg}}$ and $f_{\text{K, Reg}}$ in downstream protein-ligand binding affinity datasets (such as PDBbind). The right panel of Fig. 2 shows how the transferred model predicts the Ki value for a protein-ligand complex from PDBbind (PDB ID=3g2y).

3.2 Shared Bottom Encoder

For large-scale pre-training, a simple and effective backbone model is of utmost importance. Thus, we design the shared bottom encoder based only on vanilla GNN models. To simplify, we assume the input of the shared bottom encoder is a 3-tuple (P, L, C) , indicating a protein P , a ligand L , and their binding conformation C .

Representing Protein-Ligand Complex as Multi-Graphs The input protein-ligand complex (P, L, C) is processed into three graphs — a ligand graph, a protein graph, and a protein-ligand interaction graph. We formally define the three graphs as follows:

Definition 3 (Ligand Graph). A ligand graph, denoted by $\mathcal{G}^L = (\mathcal{V}^L, \mathcal{E}^L)$, is constructed from the input ligand L . \mathcal{V}^L is the node set where node i represents the i -th atom in the ligand. Each node i is also associated with (1) atom coordinate c_i^L retrieved from the binding conformation C and (2) atom feature vector x_i^L . The edge set \mathcal{E}^L is constructed according to the spatial distances among atoms. More formally, the edge set is defined to be

$$\mathcal{E}^L = \left\{ (i, j) : \left\| c_i^L - c_j^L \right\|_2 < \text{cut}^L, \forall i, j \in \mathcal{V}^L \right\}, \quad (6)$$

where cut^L is a distance threshold, and each edge $(i, j) \in \mathcal{E}^L$ is associated with an edge feature vector e_{ij}^L . The node and edge features are obtained by Open Babel [70].

Definition 4 (Protein Graph). A protein graph, denoted by $\mathcal{G}^P = (\mathcal{V}^P, \mathcal{E}^P)$, is constructed from the input protein P . \mathcal{V}^P is the node set where the node i represents the i -th residue in the protein. Each

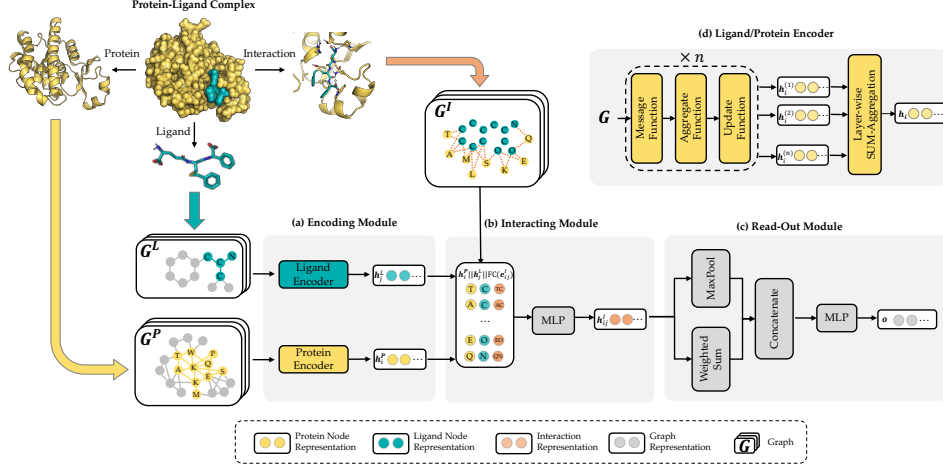


Figure 3: Shared bottom encoder of MBP. It contains three modules: (a) encoding module, (b) interacting module, and (c) read-out module. (d) shows the detailed GNN model of the ligand/protein encoder in the encoding module.

node v_i^P is also associated with (1) the alpha carbon coordinate of the i -th residue c_i^P retrieved from the binding conformation C and (2) the residue feature vector \mathbf{x}_i^P . The edge set \mathcal{E}^P is constructed according to the spatial distances among atoms. More formally, the edge set is defined to be

$$\mathcal{E}^P = \left\{ (i, j) : \left\| c_i^P - c_j^P \right\|_2 < cut^P, \forall i, j \in \mathcal{V}^P \right\}, \quad (7)$$

where cut^P is a distance threshold, and each edge $(i, j) \in \mathcal{E}^P$ is associated with an edge feature vector \mathbf{e}_{ij}^P . The node and edge features are obtained following [71].

Definition 5 (Interaction Graph). The protein-ligand interaction graph $\mathcal{G}^I = (\mathcal{V}^P, \mathcal{V}^L, \mathcal{E}^I)$ is a bipartite graph constructed based on the protein-ligand complex, whose nodes set are the union of protein residues \mathcal{V}^P and ligand atoms \mathcal{V}^L . The edge set \mathcal{E}^I models the protein-ligand interactions according to spatial distances. More formally,

$$\mathcal{E}^I = \left\{ (i, j) : \left\| c_i^P - c_j^L \right\|_2 < cut^I, \forall i \in \mathcal{V}^P, j \in \mathcal{V}^L \right\}, \quad (8)$$

where cut^I is a spatial distance threshold for interaction, and each edge $(i, j) \in \mathcal{E}^I$ is associated with an edge feature vector \mathbf{e}_{ij}^I . The edge features are obtained following [71].

When constructing multi-graphs, we follow previous work[48; 72; 73; 74; 75; 76; 9] and set the distance thresholds as $cut^L = 5\text{\AA}$, $cut^P = 8\text{\AA}$ and $cut^I = 12\text{\AA}$, respectively. Limited by space, we defer the more detailed multi-graph generation pseudo-code to Appendix B.

Encoding Module (Ligand/Protein Encoder) Having represented the protein-ligand complex as multi-graphs, we respectively feed the ligand graph \mathcal{G}^L and the protein graph \mathcal{G}^P into the ligand encoder and the protein encoder, aiming to extract informative node representations. More formally, taking \mathcal{G}^L and \mathcal{G}^P as inputs, we have

$$\mathbf{H}^L = \text{GNN}(\mathcal{G}^L) \text{ and } \mathbf{H}^P = \text{GNN}(\mathcal{G}^P). \quad (9)$$

Here \mathbf{H}^L is the ligand embedding matrix of shape $|\mathcal{V}^L| \times d$. And the i -th row of \mathbf{H}^L , denoted by \mathbf{h}_i^L , represents the embedding of the i -th ligand atom. Similarly, \mathbf{H}^P is the protein embedding matrix of shape $|\mathcal{V}^P| \times d$. And the i -th row of \mathbf{H}^P , denoted by \mathbf{h}_i^P , represents the embedding of the i -th protein residue.

Encoders used here can be any GNN model, such as GCN, GAT, GIN, EGNN, AttentiveFP, etc. Here we briefly review GNNs following the message-passing paradigm following [77] and [78]. For simplicity and convenience, we assume that the GNN operates on graph \mathcal{G} with node features \mathbf{x}_i and edge features \mathbf{e}_{ij} , and temporarily ignore whether it is a ligand or protein graph. The message-passing process runs for several iterations. At the ℓ -th iteration, the message-passing is defined according to a message function M_ℓ , an aggregation function AGGREGATOR_ℓ , and an update function U_ℓ . The

embedding $\mathbf{h}_i^{(\ell)}$ of node i is updated via its message $\mathbf{m}_i^{(\ell+1)}$:

$$\begin{aligned}\mathbf{m}_i^{(\ell+1)} &= \text{AGGREGATOR}_\ell \left(\left\{ M_\ell \left(\mathbf{h}_i^{(\ell)}, \mathbf{h}_j^{(\ell)}, \mathbf{e}_{ij} \right), j \in \mathcal{N}(i) \right\} \right), \\ \mathbf{h}_i^{(\ell+1)} &= U_\ell \left(\mathbf{h}_i^{(\ell)}, \mathbf{m}_i^{(\ell+1)} \right),\end{aligned}\quad (10)$$

where $\mathcal{N}(i)$ is the neighbors of node i . Finally, after n iterations of message passing, we sum up the node representations of each layer to get the final node representation, i.e., $\mathbf{h}_i = \sum_{\ell=1}^n \mathbf{h}_i^{(\ell)}$. The GNNs with layer-wise aggregation are also known as jumping knowledge networks [79].

Interacting Module After extracting ligand atom embedding \mathbf{h}_i^L and protein residue embedding \mathbf{h}_j^P from the encoding module, the interacting module is designed to conduct knowledge fusion according to the protein-ligand interaction graph. For each protein-ligand interaction edge $(i, j) \in \mathcal{E}^I$, we define its interaction embedding as the concatenation of the protein residue embedding \mathbf{h}_i^P , ligand atom embedding \mathbf{h}_j^L , and transformed edge features. More formally,

$$\mathbf{h}_{ij}^I = \text{MLP} \left(\mathbf{h}_i^P \parallel \mathbf{h}_j^L \parallel \text{FC}(\mathbf{e}_{ij}^I) \right), \quad (11)$$

where \parallel is the concatenation operator, MLP is a multilayer perceptron, and FC is a fully-connected layer.

Read-Out Module After obtaining interaction embeddings \mathbf{h}_{ij}^I for each protein-ligand interaction edge $(i, j) \in \mathcal{E}^I$, we further apply an attention-based weighted sum operation to read out a global embedding for the whole protein-ligand complex:

$$\mathbf{o}_{\text{sum}} = \sum_{(i,j) \in \mathcal{E}^I} \tanh(\mathbf{w}^\top \mathbf{h}_{ij}^I) \mathbf{h}_{ij}^I, \quad (12)$$

where \mathbf{w} is the attention vector, \tanh is the hyperbolic tangent function. Besides, a global maximum pooling operation is adopted to highlight the most informative interaction embedding, s.t., $\mathbf{o}_{\text{max}} = \text{MaxPool}(\mathbf{h}_{ij}^I)$. We concatenate the above two graph-level embedding to form the final graph embedding for the protein-ligand complex (P, L, C) , i.e., $\mathbf{o} = \mathbf{o}_{\text{sum}} \parallel \mathbf{o}_{\text{max}}$.

3.3 Pre-training Dataset: ChEMBL-Dock

ChEMBL-Dock is a self-constructed dataset used for pre-training MBP. The detailed ChEMBL-based curation workflow, including the data collection & cleaning step and molecular docking step, can be found in Appendix D. Here, we compare it to other commonly used protein-ligand complex datasets in terms of the label, 3D structure, protein diversity, molecular diversity, and dataset size in Fig.S1 and Table 1.

Combining the strengths of molecular docking and ChEMBL, ChEMBL-Dock provides a large-scale 3D protein-ligand complex dataset with corresponding experimental affinity labels. While the quality of the docked 3D structures of the complexes in ChEMBL-Dock is not as high as that of the 3D co-crystal structures of the protein-ligand complexes in PDBbind, ChEMBL-Dock provides a much larger number of 3D structures of protein-ligand complexes than the PDBbind database. By comparing ChEMBL-Dock and CrossDocked, two datasets generated through molecular docking, it is evident that ChEMBL-Dock exhibits a higher molecular diversity than CrossDocked, suggesting its potential to provide a more comprehensive dataset for drug discovery research.

Table 1: Overview of data represented in PDBbind, CrossDocked, and ChEMBL-Dock, respectively.

	PDBbind	CrossDocked	ChEMBL-Dock
Protein	3,890	2,922	963
Ligand	15,193	13,780	200,728
Protein-ligand pair	19,443	/	313,224
Pose	19,443	22,584,102	2,819,016
Assay	/	/	21,686

4 Experiments

4.1 Experimental Setup

Downstream Datasets. Two publicly available datasets are used to comprehensively evaluate the performance of models.

- **PDBbind v2016** [13] is a famous benchmark for evaluating the performance of models in predicting PLBA. The dataset includes three overlapping subsets: the general set (13,283 3D protein-ligand complexes), the refined set (4,057 complexes selected out of the general set with better quality), and the core set (290 complexes selected as the highest quality benchmark for testing). We refer to the difference between the refined and core subsets (3,767 complexes) as the refined set for convenience. The general set contains IC50 data and K data, while the refined set and core only contain K data. In this paper, the core set is used as the test set, and we train models on the refined set or the general set.
- **CSAR-HiQ** [46] is a publicly available dataset of 3D protein-ligand complexes with associated experimental affinity labels. Data included in CSAR-HiQ are K data. When training models on the refined set of PDBbind, CSAR-HiQ is typically used to evaluate the generalization performance of the model [9]. In this paper, we create an independent test set of 135 samples based on CSAR-HiQ by removing samples that already exist in the PDBbind v2016 refined set.

Baselines. We mainly compare MBP with four families of methods. The first family is machine learning-based methods such as Linear Regression (LR), Support Vector Regression (SVR), and RF-Score [80]. The second family is CNN-based methods, including Pafnucy [40] and OnionNet [6]. The third family of baselines is GraphDTA [41] methods, including GCN, GAT, GIN, GAT-GCN. The fourth family of baselines is GNN-based methods containing SGCN [42], GNN-DTI [81], DMPNN [82], MAT [15], DimeNet [43], CMPNN [44], IGN [8], and SIGN [9]. In addition, the recent molecular docking method TANKBind [47] and molecular pre-training method Transformer-M [83] are also compared as they have been applied to perform PLBA predictions.

Evaluation Metrics. Root Mean Square Error (RMSE), Mean Absolute Error (MAE), Standard Deviation (SD), and Pearson’s correlation coefficient (R) are used to evaluate the performance of PLBA prediction [9]. The definition of these metrics can be found in Appendix C.

Training Parameter Settings. The models were trained using Adam [84] with an initial learning rate of 10^{-3} and an L_2 regularization factor of 10^{-6} . The learning rate was scaled down by 0.6 if no drop in training loss was observed for 10 consecutive epochs. For pre-training, the number of training epochs was set to 100, while for fine-tuning, the number of training epochs was set to 1000 with an early stopping rule of 70 epochs if no improvement in the validation performance was observed.

4.2 Experimental Results

In this work, we employ five different GNNs in the shared bottom encoder of MBP, which are denoted as MBP-X (where X corresponds to the GNN used) for distinction. For example, MBP-GCN denotes the MBP model using GCN in its shared bottom encoder. Unless specified otherwise, AttentiveFP is used as the default GNN in MBP.

Overall Performance Comparison on PDBbind core set and CSAR-HiQ. We first fine-tune MBP on the PDBbind refined set and report the test performance averaged over five repetitions for each method on the PDBbind core set and CSAR-HiQ set in Table 2. It can be observed that MBP achieves the best performance across all metrics of the two publicly available datasets. In particular, MBP-AttentiveFP and MBP-EGNN outperforms all competing methods on the PDBbind core set. Compared with SIGN, which the previous SOTA method [9], MBP-AttentiveFP achieving an improvement of 4.0%, 2.7%, 6.3%, and 3.5% on RMSE, MAE, SD, and R, respectively. And on the CSAR-HiQ dataset, MBP-AttentiveFP also achieves results superior to the other competing methods. For instance, it attains more than 6.3%, 6.6%, 10.1%, and 4.9% on RMSE, MAE, SD, and R gain compared to SIGN. Both MBP-EGNN and MBP-AttentiveFP surpass the previous best method, SIGN, and are the best two methods in the current results. In addition, it is worth noting that MBP with even the simplest GNN models (e.g., GCN) outperforms SIGN on the CSAR-HiQ dataset. This indicates that the proposed multi-task pre-training framework is able to improve the capacity and generalization of the backbone model in the PLBA prediction problem. To further evaluate the generalization performance of the proposed model, we conduct an extra experiment on the PDBbind general set. As shown in Fig. 4, comparing to all baselines, MBP achieves the best performance in terms of both RMSE and MAE.

For the molecular docking method TANKBind and the molecular pre-training method Transformer-M, we conducted experiments by adhering to the reported settings of these methods and fine-tuned our MBP model accordingly to ensure a fair comparison. Due to the variations in experimental settings and limited space, we provide a detailed comparison setting and results in Appendix E. The outcomes

Table 2: Test performance comparison on the PDBbind v2016 core set and the CSAR-HiQ dataset. The mean RMSE, MAE, SD, and R (std) over 3 repetitions are reported. The best two results are highlighted in **bold**.

Method	PDBbind core set				CSAR-HiQ dataset			
	RMSE↓	MAE↓	SD↓	R↑	RMSE↓	MAE↓	SD↓	R↑
ML-based	LR	1.675 (0.000)	1.358 (0.000)	1.612 (0.000)	0.671 (0.000)	2.071 (0.000)	1.622 (0.000)	1.973 (0.000)
	SVR	1.555 (0.000)	1.264 (0.000)	1.493 (0.000)	0.727 (0.000)	1.995 (0.000)	1.553 (0.000)	1.911 (0.000)
	RF-Score	1.446 (0.008)	1.161 (0.007)	1.335 (0.010)	0.789 (0.003)	1.947 (0.012)	1.466 (0.009)	1.796 (0.020)
CNN-based	Pafnucy	1.585 (0.013)	1.284 (0.021)	1.563 (0.022)	0.695 (0.011)	1.939 (0.103)	1.562 (0.094)	1.885 (0.071)
	OnionNet	1.407 (0.034)	1.078 (0.028)	1.391 (0.038)	0.768 (0.014)	1.927 (0.071)	1.471 (0.031)	1.877 (0.097)
GraphDTA	GCN	1.735 (0.034)	1.343 (0.037)	1.719 (0.027)	0.613 (0.016)	2.324 (0.079)	1.732 (0.065)	2.302 (0.061)
	GAT	1.765 (0.026)	1.354 (0.033)	1.740 (0.027)	0.601 (0.016)	2.213 (0.053)	1.651 (0.061)	2.215 (0.050)
	GIN	1.640 (0.044)	1.261 (0.044)	1.621 (0.036)	0.667 (0.018)	2.158 (0.074)	1.624 (0.058)	2.156 (0.088)
	GAT-GCN	1.562 (0.022)	1.191 (0.016)	1.558 (0.018)	0.697 (0.008)	1.980 (0.055)	1.493 (0.046)	1.969 (0.057)
GNN-based	SGCN	1.583 (0.033)	1.250 (0.036)	1.582 (0.320)	0.686 (0.015)	1.902 (0.063)	1.472 (0.067)	1.891 (0.077)
	GNN-DTI	1.492 (0.025)	1.192 (0.032)	1.471 (0.051)	0.736 (0.021)	1.972 (0.061)	1.547 (0.058)	1.834 (0.090)
	DMPNN	1.493 (0.016)	1.188 (0.009)	1.489 (0.014)	0.729 (0.006)	1.886 (0.026)	1.488 (0.054)	1.865 (0.035)
	MAT	1.457 (0.037)	1.154 (0.037)	1.445 (0.033)	0.747 (0.013)	1.879 (0.065)	1.435 (0.058)	1.816 (0.083)
	DimeNet	1.453 (0.027)	1.138 (0.026)	1.434 (0.023)	0.752 (0.010)	1.805 (0.036)	1.338 (0.026)	1.798 (0.027)
	CMPNN	1.408 (0.028)	1.117 (0.031)	1.399 (0.025)	0.765 (0.009)	1.839 (0.096)	1.411 (0.064)	1.767 (0.103)
	IGN	1.519 (0.055)	1.187 (0.042)	1.513 (0.052)	0.718 (0.023)	2.051 (0.077)	1.604 (0.043)	1.834 (0.095)
	SIGN	1.316 (0.031)	1.027 (0.025)	1.312 (0.035)	0.797 (0.012)	1.735 (0.031)	1.327 (0.040)	1.709 (0.044)
Ours	MBP-GCN	1.333 (0.019)	1.056 (0.011)	1.306 (0.018)	0.800 (0.006)	1.718 (0.044)	1.348 (0.025)	1.659 (0.048)
	MBP-GIN	1.375 (0.031)	1.088 (0.026)	1.352 (0.044)	0.783 (0.016)	1.748 (0.028)	1.391 (0.026)	1.664 (0.050)
	MBP-GAT	1.393 (0.017)	1.122 (0.007)	1.367 (0.023)	0.778 (0.008)	1.703 (0.039)	1.317 (0.041)	1.606 (0.022)
	MBP-EGNN	1.298 (0.029)	1.023 (0.025)	1.262 (0.033)	0.815 (0.011)	1.649 (0.045)	1.242 (0.036)	1.548 (0.055)
	MBP-AttentiveFP	1.263 (0.023)	0.999 (0.024)	1.229 (0.026)	0.825 (0.008)	1.624 (0.037)	1.240 (0.038)	1.536 (0.052)

¹ The result of IGN was obtained by repeating the protocol provided by its authors. The other results were taken from [9].

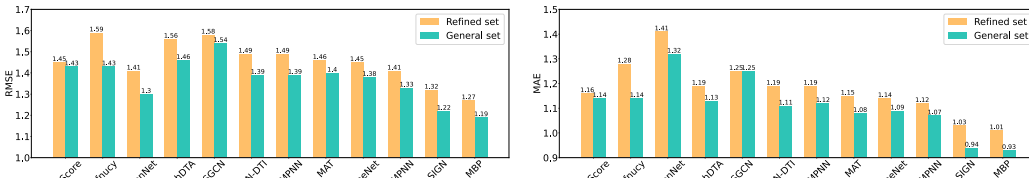


Figure 4: Performance improvements of baselines and MBP on the PDBbind benchmark when training on general set.

presented in Table S1 and Table S2 demonstrate the effectiveness and competitiveness of MBP, even when compared to these powerful methods.

4.3 Ablation Studies

In this section, we conduct extensive ablation studies to investigate the role of different components in MBP. In ablation studies, all MBP models are fine-tuned on the PDBbind refined set.

Multi-Task Learning Objectives. We perform an ablation study to investigate the effect of multi-task learning. Table 3 shows the results of our MBP with different learning tasks. We have two main observations:

- **Regarding regression tasks and ranking tasks**, we find that on both PDBbind core set and independent CSAR-HiQ set, MBP with a combination of both regression and ranking tasks can always outperform MBP with only regression or ranking tasks, indicating the power of ensembling regression and bioassay-specific ranking.
- **Regarding IC50 tasks and K tasks**, we also find that MBP pre-trained with both IC50 and K tasks is better than that using only IC50 or K tasks. This implies that MBP is able to learn the task correlation between IC50 and K data from ChEMBL and transfer the knowledge to the PDBbind core set, which only contains Ki/Kd data.

These results justify the effectiveness of the multi-task learning objectives designed in MBP.

GNN Used in Shared Bottom Encoder. As shown in Table 2, we benchmark and compare MBP with different GNNs in the shared bottom encoder. We choose five popular GNN models — GCN, GIN, GAT, EGNN, and AttentiveFP. EGNN and AttentiveFP are able to capture the 3D structure of biomolecules, while GCN, GIN, and GAT are mainly designed for general graphs which can not capture structural information directly. We have two interesting observations. Firstly, all GNN models, even the vanilla GCN, achieve comparable or better performance than previous methods. For example, MBP-GCN achieves RMSE of 1.718 on the CSAR-HiQ set, slightly better than SIGN’s

Table 3: Ablation study of MBP with different pre-training tasks. The mean RMSE, MAE, SD, and R (std) over 5 repetitions are reported. The best two results are highlighted in **bold**.

Regression		Ranking		PDBbind core set				CSAR-HiQ set			
IC50	K	IC50	K	RMSE↓	MAE↓	SD↓	R↑	RMSE↓	MAE↓	SD↓	R↑
				1.377 (0.045)	1.075 (0.040)	1.366 (0.042)	0.778 (0.015)	1.661 (0.028)	1.270 (0.035)	1.629 (0.043)	0.777 (0.008)
✓				1.364 (0.009)	1.077 (0.005)	1.351 (0.010)	0.784 (0.004)	1.693 (0.038)	1.293 (0.031)	1.628 (0.036)	0.761 (0.011)
	✓	✓		1.418 (0.036)	1.120 (0.041)	1.398 (0.037)	0.766 (0.014)	1.787 (0.082)	1.386 (0.062)	1.756 (0.062)	0.714 (0.024)
✓			✓	1.315 (0.011)	1.055 (0.010)	1.268 (0.014)	0.813 (0.005)	1.690 (0.037)	1.268 (0.048)	1.470 (0.052)	0.764 (0.016)
	✓			1.292 (0.025)	1.018 (0.023)	1.267 (0.032)	0.813 (0.011)	1.704 (0.132)	1.254 (0.053)	1.586 (0.060)	0.746 (0.058)
		✓	✓	1.372 (0.029)	1.096 (0.032)	1.365 (0.036)	0.779 (0.013)	1.659 (0.008)	1.294 (0.026)	1.601 (0.032)	0.771 (0.010)
✓			✓	1.283 (0.023)	1.017 (0.014)	1.255 (0.032)	0.817 (0.010)	1.637 (0.018)	1.233 (0.036)	1.580 (0.008)	0.788 (0.011)
✓	✓			1.287 (0.025)	1.027 (0.024)	1.254 (0.031)	0.817 (0.010)	1.662 (0.048)	1.269 (0.032)	1.544 (0.058)	0.789 (0.018)
		✓	✓	1.325 (0.010)	1.048 (0.011)	1.307 (0.013)	0.800 (0.044)	1.674 (0.045)	1.293 (0.033)	1.616 (0.049)	0.766 (0.016)
✓	✓	✓	✓	1.263 (0.023)	0.999 (0.024)	1.229 (0.026)	0.825 (0.008)	1.624 (0.037)	1.240 (0.038)	1.536 (0.052)	0.791 (0.016)

1.735. Secondly, GNNs that explicitly capture 3D structure information (EGNN and AttentiveFP) outperform GNNs designed for general graphs (GCN, GAT, GIN).

Hyper-Parameter Studies.

We ablate the weight coefficient λ of regression loss in MBP, which is crucial to the performance of MBP. Intuitively, too small a λ may hurt the ability to predict binding affinity, while too large a λ may aggravate the label noise problem. We vary the weight coefficients λ from $\{0, 0.01, 0.1, 0.3, 1.0\}$, and then depict the tendency curves of the test RMSE w.r.t. λ in Fig. 5. As expected, too large or too small a weight coefficient leads to worse performance in different multi-task settings (i.e., IC50 tasks, K tasks, and IC50+K tasks).

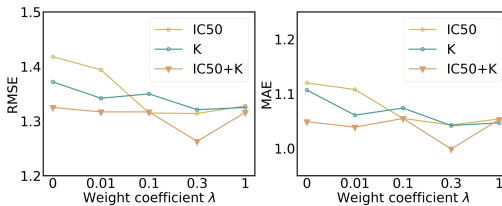


Figure 5: Test RMSE and MAE of MBP on the PDBbind core set with varying weight coefficients λ of the regression loss.

5 Conclusion

Protein-ligand binding affinity (PLBA) is a critical measure in drug discovery. However, the limited availability of high-quality training data and the variety and noise of PLBA labels pose difficulties in improving the performance of these models through pre-training. In this paper, we introduce the ChEMBL-Dock dataset, which contains 313,224 3D protein-ligand complexes with experimental PLBA labels. Based on this dataset, we proposed the MBP method that addresses the label variety and noise problems through multi-task learning and assay-specific ranking tasks.

References

- [1] Bruno Rizzuti and Fedora Grande. Chapter 14 - virtual screening in drug discovery: a precious tool for a still-demanding challenge. In Angel L. Pey, editor, *Protein Homeostasis Diseases*, pages 309–327. Academic Press, 2020.
- [2] Sangmin Seo, Jonghwan Choi, Sanghyun Park, and Jaegyeon Ahn. Binding affinity prediction for protein–ligand complex using deep attention mechanism based on intermolecular interactions. *BMC Bioinformatics*, 22, 2021.
- [3] Laurent Jacob and Jean-Philippe Vert. Protein-ligand interaction prediction: an improved chemogenomics approach. *Bioinformatics*, 24:2149 – 2156, 2008.
- [4] Yuqing Deng and Benoît Roux. Computations of standard binding free energies with molecular dynamics simulations. *The Journal of Physical Chemistry B*, 113(8):2234–2246, 2009.
- [5] Marta M. Stepniewska-Dziubinska, Piotr Zielenkiewicz, and Paweł Siedlecki. Development and evaluation of a deep learning model for protein–ligand binding affinity prediction. *Bioinformatics*, 34:3666 – 3674, 2018.
- [6] Liangzhen Zheng, Jingrong Fan, and Yuguang Mu. Onionnet: a multiple-layer intermolecular-contact-based convolutional neural network for protein–ligand binding affinity prediction. *ACS Omega*, 4:15956 – 15965, 2019.
- [7] Lifan Chen, Xiaoqin Tan, Dingyan Wang, Feisheng Zhong, Xiaohong Liu, Tianbiao Yang, Xiaomin Luo, Kaixian Chen, Hualiang Jiang, Mingyue Zheng, and Arne Elofsson. Transformer-cpi: improving compound-protein interaction prediction by sequence-based deep learning with self-attention mechanism and label reversal experiments. *Bioinformatics*, 2020.
- [8] Dejun Jiang, Chang-Yu Hsieh, Zhenxing Wu, Yu Kang, Jike Wang, Ercheng Wang, Ben Liao, Chao Shen, Lei Xu, Jian Wu, et al. Interactiongraphnet: A novel and efficient deep graph representation learning framework for accurate protein–ligand interaction predictions. *Journal of medicinal chemistry*, 2021.
- [9] Shuangli Li, Jingbo Zhou, Tong Xu, Liang Huang, Fan Wang, Haoyi Xiong, Weili Huang, Dejing Dou, and Hui Xiong. Structure-aware interactive graph neural networks for the prediction of protein-ligand binding affinity. *KDD '21*, 2021.
- [10] José Jiménez, Miha Skalic, Gerard Martinez-Rosell, and Gianni De Fabritiis. Kdeep: protein–ligand absolute binding affinity prediction via 3d-convolutional neural networks. *Journal of chemical information and modeling*, 58(2):287–296, 2018.
- [11] Hussein Hassan-Harrirou, Ce Zhang, and Thomas Lemmin. Rosenet: improving binding affinity prediction by leveraging molecular mechanics energies with an ensemble of 3d convolutional neural networks. *Journal of chemical information and modeling*, 60(6):2791–2802, 2020.
- [12] Derek Jones, Hyojin Kim, Xiaohua Zhang, Adam T. Zemla, Garrett Stevenson, W. F. Drew Bennett, Daniel A. Kirshner, Sergio E. Wong, Felice C. Lightstone, and Jonathan E. Allen. Improved protein-ligand binding affinity prediction with structure-based deep fusion inference. *Journal of chemical information and modeling*, 2020.
- [13] Zhihai Liu, Minyi Su, Li Han, Jie Liu, Qifan Yang, Yan Li, and Renxiao Wang. Forging the basis for developing protein-ligand interaction scoring functions. *Accounts of chemical research*, 50 2:302–309, 2017.
- [14] Zaixi Zhang, Qi Liu, Hao Wang, Chengqiang Lu, and Chee-Kong Lee. Motif-based graph self-supervised learning for molecular property prediction. In *NeurIPS '21*, volume 34, pages 15870–15882, 2021.
- [15] Łukasz Maziarka, Tomasz Danel, Sławomir Mucha, Krzysztof Rataj, Jacek Tabor, and Stanisław Jastrzębski. Molecule attention transformer. *arXiv preprint arXiv:2002.08264*, 2020.
- [16] Yu Rong, Yatao Bian, Tingyang Xu, Weiyang Xie, Ying WEI, Wenbing Huang, and Junzhou Huang. Self-supervised graph transformer on large-scale molecular data. In *NeurIPS '20*, pages 12559–12571, 2020.

- [17] Jinhua Zhu, Yingce Xia, Lijun Wu, Shufang Xie, Tao Qin, Wen gang Zhou, Houqiang Li, and Tie-Yan Liu. Unified 2d and 3d pre-training of molecular representations. *KDD '22*, 2022.
- [18] Xiaomin Fang, Lihang Liu, Jieqiong Lei, Donglong He, Shanzhuo Zhang, Jingbo Zhou, Fan Wang, Hua Wu, and Haifeng Wang. Chemrl-gem: Geometry enhanced molecular representation learning for property prediction. *Nat. Mach. Intell.*, 4:127–134, 2021.
- [19] Serbulent Unsal, Heval Atas, Muammer Albayrak, Kemal Turhan, Aybar Can Acar, and Tunca Dogan. Learning functional properties of proteins with language models. *Nat. Mach. Intell.*, 4:227–245, 2022.
- [20] Roshan M Rao, Jason Liu, Robert Verkuil, Joshua Meier, John Canny, Pieter Abbeel, Tom Sercu, and Alexander Rives. Msa transformer. In *ICML '21*, pages 8844–8856, 2021.
- [21] Ahmed Elnaggar, Michael Heinzinger, Christian Dallago, Ghalia Rihawi, Yu Wang, Llion Jones, Tom Gibbs, Tamas Feher, Christoph Angerer, Debsindhu Bhowmik, and Burkhard Rost. Prottrans: Towards cracking the language of lifes code through self-supervised deep learning and high performance computing. *TPAMI '21*, 44(10), 2021.
- [22] Anna Gaulton, Louisa J. Bellis, A. Patrícia Bento, Jon Chambers, Mark Davies, Anne Hersey, Yvonne Light, Shaun McGlinchey, David Michalovich, Bissan Al-Lazikani, and John P. Overington. ChEMBL: a large-scale bioactivity database for drug discovery. *Nucleic Acids Research*, 40:D1100 – D1107, 2011.
- [23] Tiqing Liu, Yuhmei Lin, Xin Wen, Robert N. Jorissen, and Michael K. Gilson. Bindingdb: a web-accessible database of experimentally determined protein–ligand binding affinities. *Nucleic Acids Research*, 35:D198 – D201, 2006.
- [24] Hongyu Luo, Yingfei Xiang, Xiaomin Fang, Wei Lin, Fan Wang, Hua Wu, and Haifeng Wang. Batchdta: implicit batch alignment enhances deep learning-based drug–target affinity estimation. *Briefings in Bioinformatics*, 23(4), 2022.
- [25] George Papadatos, Anna Gaulton, Anne Hersey, and John P Overington. Activity, assay and target data curation and quality in the ChEMBL database. *Journal of computer-aided molecular design*, 29:885–896, 2015.
- [26] Michael Crawshaw. Multi-task learning with deep neural networks: A survey. *arXiv preprint arXiv:2009.09796*, 2020.
- [27] Menghan Wang, Yuchen Guo, Zhen Zhao, Guangzheng Hu, Yuming Shen, Mingming Gong, and Philip H. S. Torr. Mp2: A momentum contrast approach for recommendation with pointwise and pairwise learning. In *SIGIR '22*, 2022.
- [28] Yagmur Gizem Cinar and Jean-Michel Renders. Adaptive pointwise-pairwise learning-to-rank for content-based personalized recommendation. *RecSys '20*, 2020.
- [29] Yu Lei, Wenjie Li, Ziyu Lu, and Miao Zhao. Alternating pointwise-pairwise learning for personalized item ranking. *CIKM '17*, 2017.
- [30] Thomas N. Kipf and Max Welling. Semi-supervised classification with graph convolutional networks. In *ICLR '17*, 2017.
- [31] Keyulu Xu, Weihua Hu, Jure Leskovec, and Stefanie Jegelka. How powerful are graph neural networks? In *ICLR '19*, 2019.
- [32] Petar Veličković, Guillem Cucurull, Arantxa Casanova, Adriana Romero, Pietro Liò, and Yoshua Bengio. Graph attention networks. In *ICLR '18*, 2018.
- [33] Jiaqi Han, Yu Rong, Tingyang Xu, and Wenbing Huang. Geometrically equivariant graph neural networks: A survey. *arXiv preprint arXiv:2202.07230*, 2022.
- [34] Zhaoping Xiong, Dingyan Wang, Xiaohong Liu, Feisheng Zhong, Xiaozhe Wan, Xutong Li, Zhaojun Li, Xiaomin Luo, Kaixian Chen, Hualiang Jiang, and Mingyue Zheng. Pushing the boundaries of molecular representation for drug discovery with graph attention mechanism. *Journal of medicinal chemistry*, 2020.

- [35] Holger Gohlke, Manfred Hendlich, and Gerhard Klebe. Knowledge-based scoring function to predict protein-ligand interactions. *Journal of molecular biology*, 295(2):337–356, 2000.
- [36] Oleg Trott and Arthur J Olson. Autodock vina: improving the speed and accuracy of docking with a new scoring function, efficient optimization, and multithreading. *Journal of computational chemistry*, 31(2):455–461, 2010.
- [37] Renxiao Wang, Luhua Lai, and Shaomeng Wang. Further development and validation of empirical scoring functions for structure-based binding affinity prediction. *Journal of computer-aided molecular design*, 16:11–26, 2002.
- [38] Pedro J Ballester and John BO Mitchell. A machine learning approach to predicting protein–ligand binding affinity with applications to molecular docking. *Bioinformatics*, 26(9):1169–1175, 2010.
- [39] Sarah L Kinnings, Nina Liu, Peter J Tonge, Richard M Jackson, Lei Xie, and Philip E Bourne. A machine learning-based method to improve docking scoring functions and its application to drug repurposing. *Journal of chemical information and modeling*, 51(2):408–419, 2011.
- [40] Marta M. Stepniewska-Dziubinska, Piotr Zielenkiewicz, and Paweł Siedlecki. Development and evaluation of a deep learning model for protein–ligand binding affinity prediction. *Bioinformatics*, 34:3666 – 3674, 2018.
- [41] Thin Nguyen, Hang Le, Thomas P Quinn, Tri Nguyen, Thuc Duy Le, and Svetha Venkatesh. Graphdta: predicting drug–target binding affinity with graph neural networks. *Bioinformatics*, 37(8):1140–1147, 2021.
- [42] Tomasz Danel, Przemysław Spurek, Jacek Tabor, Marek Śmieja, Łukasz Struski, Agnieszka Słowik, and Łukasz Maziarka. Spatial graph convolutional networks. In *ICONIP '20*, pages 668–675, 2020.
- [43] Johannes Gasteiger, Janek Groß, and Stephan Günnemann. Directional message passing for molecular graphs. In *ICLR '20*, 2020.
- [44] Ying Song, Shuangjia Zheng, Zhangming Niu, Zhang-Hua Fu, Yutong Lu, and Yuedong Yang. Communicative representation learning on attributed molecular graphs. In *IJCAI '20*, 2020.
- [45] Christian Kramer and Peter Gedeck. Leave-cluster-out cross-validation is appropriate for scoring functions derived from diverse protein data sets. *Journal of chemical information and modeling*, 50 11:1961–9, 2010.
- [46] James B. Dunbar, Richard D. Smith, Kelly L. Damm-Ganamet, Aqeel Ahmed, Emilio Xavier Esposito, James Delproposito, Krishnapriya Chinnaswamy, You-Na Kang, Ginger Kubish, Jason E. Gestwicki, Jeanne A. Stuckey, and Heather A. Carlson. Csar data set release 2012: Ligands, affinities, complexes, and docking decoys. *Journal of Chemical Information and Modeling*, 53:1842 – 1852, 2013.
- [47] Wei Lu, Qifeng Wu, Jixian Zhang, Jiahua Rao, Chengtao Li, and Shuangjia Zheng. TANKBind: Trigonometry-aware neural networks for drug-protein binding structure prediction. In *NeurIPS '22*, 2022.
- [48] Hannes Stärk, Octavian-Eugen Ganea, Lagnajit Pattanaik, Regina Barzilay, and T. Jaakkola. Equibind: Geometric deep learning for drug binding structure prediction. In *ICML '22*, 2022.
- [49] Xuanyu Meng, Hong-Xing Zhang, Mihaly Mezei, and Meng Cui. Molecular docking: a powerful approach for structure-based drug discovery. *Current computer-aided drug design*, 7 2:146–57, 2011.
- [50] Paul G. Francoeur, Tomohide Masuda, Jocelyn Sunseri, Andrew Jia, Richard B Iovanisci, Ian Snyder, and David Ryan Koes. Three-dimensional convolutional neural networks and a cross-docked data set for structure-based drug design. *Journal of chemical information and modeling*, 2020.

- [51] Xingang Peng, Shitong Luo, Jiaqi Guan, Qi Xie, Jian Peng, and Jianzhu Ma. Pocket2mol: Efficient molecular sampling based on 3d protein pockets. In *ICML '22*, 2022.
- [52] Gengmo Zhou, Zhifeng Gao, Qiankun Ding, Hang Zheng, Hongteng Xu, Zhewei Wei, Linfeng Zhang, and Guolin Ke. Uni-mol: A universal 3d molecular representation learning framework. In *ICLR '23*, 2023.
- [53] Zhe Cao, Tao Qin, Tie-Yan Liu, Ming-Feng Tsai, and Hang Li. Learning to rank: from pairwise approach to listwise approach. In *ICML '07*, 2007.
- [54] Marius Köppel, Alexander Segner, Martin Wagener, Lukas Pensel, Andreas Karwath, and Stefan Kramer. Pairwise learning to rank by neural networks revisited: Reconstruction, theoretical analysis and practical performance. In *ECML/PKDD '19*, page 237–252, 2019.
- [55] Tie-Yan Liu et al. Learning to rank for information retrieval. *Foundations and Trends® in Information Retrieval*, 3(3):225–331, 2009.
- [56] Steffen Rendle, Christoph Freudenthaler, Zeno Gantner, and Lars Schmidt-Thieme. Bpr: Bayesian personalized ranking from implicit feedback. In *UAI '09*, pages 452–461, 2009.
- [57] Chris Burges, Tal Shaked, Erin Renshaw, Ari Lazier, Matt Deeds, Nicole Hamilton, and Greg Hullender. Learning to rank using gradient descent. In *ICML '05*, pages 89–96, 2005.
- [58] Zhaohui Zheng, Keke Chen, Gordon Sun, and Hongyuan Zha. A regression framework for learning ranking functions using relative relevance judgments. In *SIGIR '07*, pages 287–294, 2007.
- [59] Ching-Pei Lee and Chih-Jen Lin. Large-scale linear ranksvm. *Neural computation*, 26(4):781–817, 2014.
- [60] CI Bliss. Some principles of bioassay. *American Scientist*, 45(5):449–466, 1957.
- [61] Greg Landrum, Paolo Tosco, Brian Kelley, Ric, sriniker, gedec, Riccardo Vianello, NadineSchneider, Eisuke Kawashima, Andrew Dalke, David Cosgrove, Dan N, Gareth Jones, Brian Cole, Matt Swain, Samo Turk, AlexanderSavelyev, Alain Vaucher, Maciej Wójcikowski, Ichiru Take, Daniel Probst, Kazuya Ujihara, Vincent F. Scalfani, guillaume godin, Axel Pahl, Francois Berenger, JLVarjo, strets123, JP, and DoliathGavid. rdkit/rdkit: 2022_03_4 (q1 2022) release, July 2022.
- [62] David Ryan Koes, Matthew P. Baumgartner, and Carlos J. Camacho. Lessons learned in empirical scoring with smina from the csar 2011 benchmarking exercise. *Journal of chemical information and modeling*, 53 8:1893–904, 2013.
- [63] Rocco Meli, Garrett M Morris, and Philip Biggin. Scoring functions for protein-ligand binding affinity prediction using structure-based deep learning: A review. *Frontiers in bioinformatics*, page 57, 2022.
- [64] Nagarajan Natarajan, Inderjit S Dhillon, Pradeep K Ravikumar, and Ambuj Tewari. Learning with noisy labels. *NeurIPS '13*, 26, 2013.
- [65] R Caruana. Multitask learning: A knowledge-based source of inductive bias1. In *ICML '93*, pages 41–48, 1993.
- [66] Yongbeom Kwon, Woong-Hee Shin, Junsu Ko, and Juyong Lee. Ak-score: Accurate protein-ligand binding affinity prediction using an ensemble of 3d-convolutional neural networks. *International Journal of Molecular Sciences*, 21, 2020.
- [67] Seokhyun Moon, Wonho Zhung, Soojung Yang, Jaechang Lim, and Woo Youn Kim. Pignet: a physics-informed deep learning model toward generalized drug–target interaction predictions. *Chemical Science*, 13:3661 – 3673, 2020.
- [68] Xiangfeng Yan and Yong Liu. Graph–sequence attention and transformer for predicting drug–target affinity. *RSC Advances*, 12:29525 – 29534, 2022.

- [69] Hongmei Wang, Fang Guo, Mengyan Du, Guishen Wang, and Chen Cao. A novel method for drug-target interaction prediction based on graph transformers model. *BMC Bioinformatics*, 23, 2022.
- [70] Noel M. O’Boyle, Michaela S. Banck, Craig A. James, Chris Morley, Tim Vandermeersch, and Geoffrey R. Hutchison. Open babel: An open chemical toolbox. *Journal of Cheminformatics*, 3:33 – 33, 2011.
- [71] Octavian-Eugen Ganea, Xinyuan Huang, Charlotte Bunne, Yatao Bian, Regina Barzilay, T. Jaakkola, and Andreas Krause. Independent se(3)-equivariant models for end-to-end rigid protein docking. In *ICLR ’22*, 2022.
- [72] Johannes Klicpera, Janek Groß, and Stephan Günnemann. Directional message passing for molecular graphs. In *ICLR ’20*, 2020.
- [73] Gabriele Corso, Hannes Stärk, Bowen Jing, Regina Barzilay, and Tommi S. Jaakkola. Diffdock: Diffusion steps, twists, and turns for molecular docking. In *ICLR ’23*, 2023.
- [74] Huiling Zhang, Ying zong Huang, Zhendong Bei, Zhen Ju, Jintao Meng, Min Hao, Jingjing Zhang, Haiping Zhang, and Wenhui Xi. Inter-residue distance prediction from duet deep learning models. *Frontiers in Genetics*, 13, 2022.
- [75] Sheng Wang, S. Sun, Z. Li, Renyu Zhang, and Jinbo Xu. Accurate de novo prediction of protein contact map by ultra-deep learning model. *PLoS Computational Biology*, 13, 2016.
- [76] Ingo Muegge and Yvonne C. Martin. A general and fast scoring function for protein-ligand interactions: a simplified potential approach. *Journal of medicinal chemistry*, 42 5:791–804, 1999.
- [77] Justin Gilmer, Samuel S Schoenholz, Patrick F Riley, Oriol Vinyals, and George E Dahl. Neural message passing for quantum chemistry. In *ICML ’17*, pages 1263–1272, 2017.
- [78] William L. Hamilton, Zhitao Ying, and Jure Leskovec. Inductive representation learning on large graphs. In *NeurIPS ’17*, 2017.
- [79] Keyulu Xu, Chengtao Li, Yonglong Tian, Tomohiro Sonobe, Ken-ichi Kawarabayashi, and Stefanie Jegelka. Representation learning on graphs with jumping knowledge networks. In *ICML ’18*, pages 5453–5462, 2018.
- [80] Pedro J. Ballester and John B. O. Mitchell. A machine learning approach to predicting protein-ligand binding affinity with applications to molecular docking. *Bioinformatics*, 26 9:1169–75, 2010.
- [81] Jaechang Lim, Seongok Ryu, Kyubyong Park, Yo Joong Choe, Jiyeon Ham, and Woo Youn Kim. Predicting drug–target interaction using a novel graph neural network with 3d structure-embedded graph representation. *Journal of chemical information and modeling*, 59(9):3981–3988, 2019.
- [82] Kevin Yang, Kyle Swanson, Wengong Jin, Connor Coley, Philipp Eiden, Hua Gao, Angel Guzman-Perez, Timothy Hopper, Brian Kelley, Miriam Mathea, et al. Analyzing learned molecular representations for property prediction. *Journal of chemical information and modeling*, 59(8):3370–3388, 2019.
- [83] Shengjie Luo, Tianlang Chen, Yi Xu, Shuxin Zheng, Tie-Yan Liu, Di He, and Liwei Wang. One transformer can understand both 2d & 3d molecular data. In *ICLR ’23*, 2023.
- [84] Diederik P. Kingma and Jimmy Ba. Adam: A method for stochastic optimization. In *ICLR ’15*, 2015.
- [85] Kezhi Kong, G. Li, Mucong Ding, Zuxuan Wu, Chen Zhu, Bernard Ghanem, Gavin Taylor, and Tom Goldstein. Robust optimization as data augmentation for large-scale graphs. In *CVPR ’2022*, 2022.

A Pre-training and fine-tuning procedures

In this section, to facilitate other researchers to reproduce our results, we provide the pseudocode of MBP’s pre-training procedure and fine-tuning procedure in Algorithm 1 and Algorithm 2.

Algorithm 1: Pre-training Procedure for MBP.

Input: Pre-training set \mathcal{D}
Output: Pre-trained model parameters θ

```
1 Randomly initialize the parameter  $\theta$  of MBP;  
2 for  $iteration = 1, 2, \dots, 100$  do  
3   for each batch from training samples do  
4     Obtain protein node representations  $\mathbf{h}^P$  using protein encoder;  
5     Obtain ligand node representations  $\mathbf{h}^L$  using ligand encoder;  
6     Obtain interaction embedding  $\mathbf{h}^I$  ;  
7     Obtain graph-level embedding  $\mathbf{o}$  ;  
8     Calculate the affinity prediction  $\hat{y}$  using  $\mathbf{o}$ ;  
9     Calculate the ranking prediction  $\hat{r}$  using  $\mathbf{o}$ ;  
10    Calculate MBP overall  $L_{MBP}$ ;  
11    Update parameters  $\theta$  according to the gradient of  $L_{MBP}$ ;  
12  end  
13 end  
14 return  $\theta$ 
```

Algorithm 2: Fine-tuning Procedure for MBP.

Input: Finetuning set \mathcal{D} , Pre-trained model parameters θ
Output: Finetuned model parameters θ

```
1 for  $iteration = 1, 2, \dots, 1000$  do  
2   for each batch from training samples do  
3     Obtain protein node representations  $\mathbf{h}^P$  using protein encoder;  
4     Obtain ligand node representations  $\mathbf{h}^L$  using ligand encoder;  
5     Obtain interaction embedding  $\mathbf{h}^I$  ;  
6     Obtain graph-level embedding  $\mathbf{o}$  ;  
7     Calculate the affinity prediction  $\hat{y}$  using  $\mathbf{o}$ ;  
8     Calculate the regression loss  $L_{Reg}$ ;  
9     Update parameters  $\theta$  according to the gradient of  $L_{Reg}$ ;  
10  end  
11 end  
12 return  $\theta$ 
```

B Construction of Multi-Graph

Protein graphs and ligand graphs only contain intramolecular connections, and intermolecular connections are available in protein-ligand interaction graphs. We present the pseudocode of the construction process of multi-graph in Algorithm 3.

C Experiment Details

C.1 Hardwares

We pre-trained our model on four NVIDIA Tesla V100 GPUs (32G) and fine-tune it on a single GPU.

C.2 Parameter settings

When constructing multi-graph input, we set the intramolecular cutoff distance for ligand cut^L to 5.0Å and intramolecular cutoff distance for protein cut^P to 8.0 Å, with an intermolecular cutoff

Algorithm 3: Construction of Multi-Graph

Input: Protein-ligand complex (P, L, C) , intramolecular cutoff distance cut^L , cut^P and intermolecular cutoff distance cut^I
Output: The Multi-Graph $\mathcal{G}_m = (\mathcal{G}^L, \mathcal{G}^P, \mathcal{G}^I)$

```
1 Initialize  $\mathcal{E}^L \leftarrow \{\}$  and extract  $\mathcal{V}^L$  from ligand  $L$ ;  
2 for node pair  $(v_i, v_j \in \mathcal{V}^L \times \mathcal{V}^L)$  do  
3   Calculate distance  $d_{ij} \leftarrow \|c_i - c_j\|_2$ ;  
4   if  $d_{ij} \leq cut^L$  then  
5     Update edge set  $\mathcal{E}^L \leftarrow \mathcal{E}^L \cup (i, j)$ ;  
6   end  
7 end  
8 Initialize  $\mathcal{E}^P \leftarrow \{\}$  and extract  $\mathcal{V}^P$  from protein  $P$ ;  
9 for node pair  $(v_i, v_j \in \mathcal{V}^P \times \mathcal{V}^P)$  do  
10   Calculate distance  $d_{ij} \leftarrow \|c_i - c_j\|_2$ ;  
11   if  $d_{ij} \leq cut^P$  then  
12     Update edge set  $\mathcal{E}^P \leftarrow \mathcal{E}^P \cup (i, j)$ ;  
13   end  
14 end  
15 Initialize  $\mathcal{E}^I \leftarrow \{\}$  and extract  $\mathcal{V}^I$  from ligand  $L$  and protein  $P$ ;  
16 for node pair  $(v_i, v_j \in \mathcal{V}^L \times \mathcal{V}^P)$  do  
17   Calculate distance  $d_{ij} \leftarrow \|c_i - c_j\|_2$ ;  
18   if  $d_{ij} \leq cut^I$  then  
19     Update edge set  $\mathcal{E}^I \leftarrow \mathcal{E}^I \cup (i, j)$ ;  
20   end  
21 end  
22  $\mathcal{G}^L \leftarrow (\mathcal{V}^L, \mathcal{E}^L)$ ;  
23  $\mathcal{G}^P \leftarrow (\mathcal{V}^P, \mathcal{E}^P)$ ;  
24  $\mathcal{G}^I \leftarrow (\mathcal{V}^I, \mathcal{E}^I)$ ;  
25 return  $\mathcal{G}^L, \mathcal{G}^P, \mathcal{G}^I$ 
```

distance $cut^I=12.0\text{\AA}$. For GNN used in the shared bottom encoder of MBP, we use five different GNNs: GCN, GIN, GAT, EGNN, and AttentiveFP. The numbers of message-passing layers in GCN, GIN, GAT, EGNN, and AttentiveFP are set to 2, 3, 3, 3, 3, respectively. Lengths of node representations learned by the ligand encoder and protein encoder are both set to 128. For the auxiliary task, we set the balancing coefficient to 0.1. We use a three-layer MLP to predict PLBA and a one-layer MLP for auxiliary task prediction. The hidden layer dimensions of these two MLPs are 128.

C.3 Evaluation Metrics

Here, we give the formal formulas of the evaluation metrics mentioned in the experiments section:

$$RMSE = \sqrt{\frac{1}{|D|} \sum_{i=1}^{|D|} (\hat{y}_i - y_i)^2}, \quad (13)$$

$$MAE = \frac{1}{|D|} \sum_{i=1}^{|D|} |\hat{y}_i - y_i|, \quad (14)$$

$$SD = \sqrt{\frac{1}{|D|-1} \sum_{i=1}^{|D|} [y_i - (a + b\hat{y}_i)]^2}, \quad (15)$$

$$R = \frac{\sum_{i=1}^{|D|} (\hat{y}_i - \bar{\hat{y}})(y_i - \bar{y})}{\sqrt{\sum_{i=1}^{|D|} (\hat{y}_i - \bar{\hat{y}})^2 (y_i - \bar{y})^2}}, \quad (16)$$

where a and b are the intercepts and the slope of the regression line, respectively.

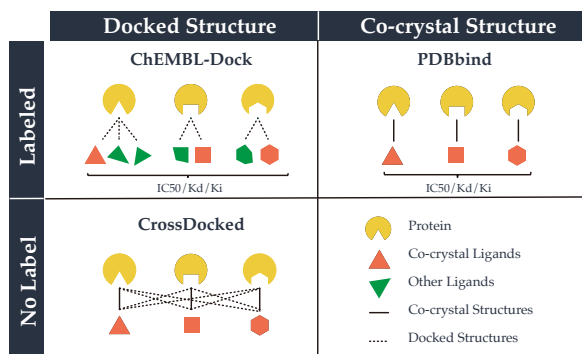


Figure S1: Comparison of ChEMBL-Dock with PDBbind and CrossDocked on label and structure.

D Curation workflow of ChEMBL-Dock

The curation workflow of ChEMBL-Dock is detailed in this section.

Data Collection and Cleaning. We first clean up the database to select high-quality PLBA data, as the bioactivity database ChEMBL covers a broad range of data, including binding, functional, absorption, distribution, metabolism, and excretion (ADME) data. The filtering criteria in ChEMBL we used are:

- STANDARD_TYPE = 'IC50'/'Ki'/'Kd' (other types of affinity, such as EC50, has limited bioassay data in ChEMBL);
- STANDARD_RELATION = '=';
- STANDARD_UNITS = 'nM';
- ASSAY_TYPE = 'B' (meaning that the data is binding data);
- TARGET_TYPE = 'SINGLE PROTEIN';
- COMPONENT_TYPE = 'PROTEIN';
- MOLECULE_TYPE = 'Small molecule';
- BAO_FORMAT = 'BAO_0000357' (meaning that in the assays, only results with single protein format were considered).

Besides the above filters, we further exclude assays with only one protein-ligand pair and assays with more than one affinity type. We then prepare the 3D structures of proteins and ligands, respectively. The 3D structures of proteins are extracted from PDBbind using their Uniprot ID, while the 3D structures of ligands are generated using RDKit. We ignore all proteins not in PDBbind and ligands that RDkit fails to generate a conformation. The final dataset comprises 313,224 protein-ligand pairs from 21,686 assays, containing a total of 231,948 IC50 protein-ligand pairs from 14,954 assays, 69,127 Ki protein-ligand pairs from 5,397 assays and 12,149 Kd protein-ligand pairs from 1,335 assays, respectively.

Molecular Docking. Molecular docking software SMINA [62] is utilized to generate 3D protein-ligand complexes. various docking strategies can be adapted to generate docking poses. Given that the proteins included in our dataset are already present in the PDBbind database, we adopt a site-specific docking approach by specifying a search space. The search space is a $22.5\text{\AA} \times 22.5\text{\AA} \times 22.5\text{\AA}$ grid box centered on the ligand of the PDBbind complex which has the same proteins. For these data, we can accurately identify the binding sites of the protein-ligand complex from the 3D structure information provided in the PDBbind database. During the docking process, SMINA generates 9 candidate poses for each protein-ligand pair. Consequently, we obtain a total of 2,819,016 poses for the 313,224 protein-ligand pairs included in our dataset. In our study, we exclusively consider the top-ranked pose for further analysis and evaluation.

Table S1: Comparison with Transformer-M on Transformer-M’s setting. The mean RMSE, MAE, SD, and R (std) over 5 repetitions are reported. The best results are highlighted in **bold**.

Method	PDBbind core set			
	RMSE↓	MAE↓	SD↓	R↑
Transformer-M	1.232 (0.013)	0.940 (0.006)	1.207 (0.007)	0.830 (0.011)
MBP	1.208 (0.011)	0.943 (0.011)	1.164 (0.017)	0.845 (0.005)

Table S2: Comparison with TANKBind on TANKBind’s setting. The mean RMSE, MAE, SD, and R (std) over 3 repetitions are reported. The best results are highlighted in **bold**.

Method	Time split test set			
	RMSE↓	MAE↓	Spearman↑	R↑
TANKBind	1.346 (0.007)	1.070 (0.019)	0.703 (0.017)	0.726 (0.007)
MBP	1.257 (0.002)	1.012 (0.016)	0.697 (0.008)	0.736 (0.001)

E Additional experimental results

In this section, we conduct a comprehensive comparative analysis between MBP, TANKBind, and Transformer-M. To ensure a fair evaluation, we base our comparison on the reported results from their papers.

E.1 Comparison with Transformer-M

We follow Transformer-M’s methodology to train and test on the PDBbind2016 dataset and use the same dataset split as Transformer-M (see https://openreview.net/forum?id=vZTp1oPV3PC¬eId=ZEa3K6qePg_formoredetails). Following Transformer-M, we employ the adversarial training method FLAG[85] during fine-tuning. We repeated the experiment five times. Our comparative analysis reveals that MBP consistently outperforms Transformer-M across multiple evaluation metrics, including RMSE, SD, and R. Notably, MBP achieves these superior results while utilizing significantly fewer model parameters, with only about 1 million parameters compared to Transformer-M’s 50 million parameters. These findings demonstrate the remarkable effectiveness of MBP in the task of PLBA prediction, surpassing the performance of the powerful molecule pre-training method, Transformer-M.

E.2 Comparison with TANKBind

In this section, we present a comparison between MBP and the molecular docking method TANKBind in the task of PLBA prediction. Specifically, we train and test MBP on the PDBbind2020 dataset, utilizing the identical dataset split (time split strategy) as employed by TANKBind. To establish statistical robustness, we repeated the experiment five times, consistent with the methodology of TANKBind. The obtained results, as summarized in Table S2, reveal a substantial advantage of MBP over TANKBind across various evaluation metrics, including RMSE, MAE, and R. Notably, MBP demonstrates a remarkable 6.6% improvement in terms of the RMSE metric when compared to TANKBind. These findings substantiate the competitiveness and effectiveness of MBP.

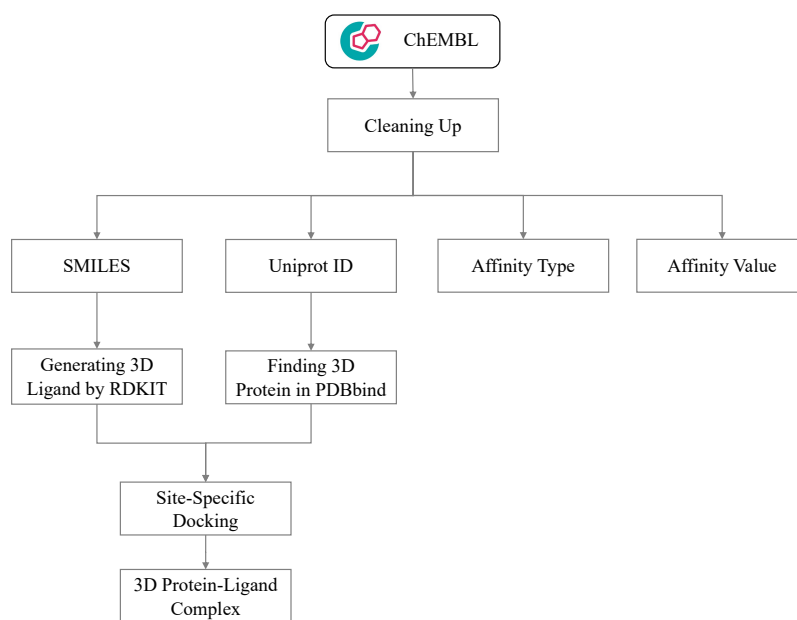


Figure S2: Construction process of ChEMBL-Dock